TRENDS IN SCIENCES 2025; 22(10): 10585
https://doi.org/10.48048/tis.2025.10585
RESEARCH ARTICLE

Microwave-Modified Reactor to Enhance the Properties and Efficacy of ZnO/GO Nanocomposites in High-Performance Methylene Blue Photocatalysis

La Agusu[1,2,*], La Ode Muhammad Darusman[3], Alimin[3], La Ode Kadidae[3], Ahmad Zaeni[3], La Ode Ahmad[3], Fadel Muhamad[3], I Wayan Sutapa[3] Yuya Ishikawa[2], Kohei Nakagawa[2], Yutaka Fujii[2], Takayuki Asano[4] and Seitaro Mitsudo[2,4]

[1]Department of Physics, Halu Oleo University, Kampus Hijau Bumi Tridharma, Anduonohu, Kendari 93232, Southeast Sulawesi, Indonesia
[2]Research Center for Development of Far-Infrared Region, University of Fukui, Fukui 9108507, Japan
[3]Department of Chemistry, Halu Oleo University, Kampus Hijau Bumi Tridharma, Anduonohu, Kendari 93232, Southeast Sulawesi, Indonesia
[4]Department of Applied Physics, Faculty of Engineering, University of Fukui, Fukui 9100017, Japan

([*]Corresponding author's e-mail: laagusu@uho.ac.id)

Received: 8 May 2025, revised: 27 May 2025, Accepted: 15 June 2025, Published: 20 July 2025

Abstract

This study investigates the synthesis and photocatalytic performance of ZnO/Graphene Oxide (GO) nanocomposites utilizing a modified microwave reactor heating technique. The ZnO/GO nanocomposites were successfully fabricated through a hydrothermal process followed by microwave irradiation. The incorporation of GO into ZnO nanoparticles significantly enhanced photocatalytic efficiency by mitigating electron-hole recombination, a notable limitation associated with pure ZnO. The application of microwave heating improved the crystallinity and uniformity of ZnO, resulting in larger particle sizes compared to those produced through conventional heating methods. This observation is observation by microstructural analysis, which indicates that the dislocation density, microstrain, and stress values in ZnO nanoparticles synthesized via conventional methods are higher than those produced by the microwave method. Furthermore, the energy density associated with conventional synthesis is lower than that achieved with the modified microwave reactor approach. Microwave heating facilitates a reduction in the band gap of the ZnO/GO composite to 2.22 eV, in contrast to the 2.62 eV observed in conventionally heated ZnO. This reduction in band gap energy enhances light absorption, thereby augmenting photocatalytic activity. Photocatalytic experiments demonstrated that ZnO/GO nanocomposites effectively degraded 87.4% of methylene blue (MB) dye under UV light and 66.6% under visible light within 50 minutes of irradiation.

Keywords: Methylene blue, Degradation, Photocatalyst, Zinc oxide, Graphene oxide, Microwave, Visible light

Introduction

Water contamination presents significant ecological challenges and disrupts environmental balance. The textile industry, identified as one of the largest contributors to this issue, produced over 700,000 tons of dyes annually in 2010, generating more than 2×10^5 tons of dye effluent during dyeing and finishing processes as a result of inefficient techniques [1,2]. Among the numerous synthetic dyes, methylene blue (MB), a triarylmethane dye, is extensively utilized across various industries, including textiles, paper, food, cosmetics, and pharmaceuticals [3]. Inadequate disposal of MB results in heightened toxicity and increased chemical oxygen demand (COD) in aquatic environments, consequently disrupting ecosystems and presenting considerable risks to both environmental and human health [4]. Therefore, the effective removal of MB dyes from wastewater is crucial for safeguarding aquatic life and ensuring the sustained availability of clean water for human consumption and use.

Numerous methodologies have been investigated for the removal of dyes from wastewater, encompassing adsorption, membrane separation, chemical oxidation, and ion exchange. Notably, photocatalysis has garnered considerable attention due to its capacity to degrade pollutants under UV-Vis light irradiation while leveraging low-cost renewable energy sources [5]. Recent advancements in nanoscience and nanotechnology have significantly enhanced photocatalytic processes, rendering them increasingly efficient and sustainable for environmental remediation [6]. Zinc oxide (ZnO) nanoparticles have emerged as promising candidates for sustainable environmental management, attributed to their superior photocatalytic and antibacterial properties [7]. Various synthesis techniques for ZnO, including spray pyrolysis [8], hydrothermal synthesis [9], and the sol-gel process [10], have been rigorously examined. Among these techniques, the modified microwave reactor heating method employed in this study has proven to be particularly effective, offering the advantage of rapid particle growth while maintaining the morphology and crystallinity of ZnO nanoparticles. This method holds significant promise for the development of high-performance ZnO nanomaterials, thereby enhancing their applicability in diverse environmental and photocatalytic applications [11].

Although ZnO and titanium dioxide (TiO_2) share similar band gap energies (~3.2 eV), ZnO is more effective than TiO_2 in degrading water pollutants due to its higher exciton binding energy (60 meV) and better electrical conductivity (~102 $\Omega^{-1}\cdot cm^{-1}$) [12]. The higher exciton binding energy enhances the stability of photogenerated electron-hole pairs, reducing recombination and increasing the availability of charge carriers (electrons and holes) for redox reactions at the catalyst surface. Meanwhile, the improved electrical conductivity facilitates faster charge transport, ensuring the efficient migration of carriers to active sites. Together, these properties enhance charge utilization, leading to faster degradation kinetics under UV light. Furthermore, these intrinsic advantages make ZnO a promising candidate for visible-light-driven photocatalysis when modified through doping or heterojunction engineering, as they help sustain charge separation and photocatalytic activity across a broader spectrum of light. However, the main limitation of ZnO photocatalysis is electron-hole recombination. To overcome this problem, researchers have focused on improving its performance by incorporating carbon-based nanomaterials, specifically graphene oxide (GO). The selection of GO over other carbon-based materials (e.g., rGO or CNTs) stems from its unique balance of oxygen functional groups and electrical properties, which synergistically address ZnO's electron-hole recombination. While rGO offers higher conductivity, its reduced oxygen content diminishes interfacial interactions with ZnO, limiting charge transfer pathways. In contrast, GO retains abundant epoxy, hydroxyl, and carboxyl groups that anchor ZnO nanoparticles via covalent bonding, preventing aggregation, and also act as electron reservoirs, prolonging charge separation. CNTs, though conductive, lack sufficient functional groups for uniform ZnO dispersion and may introduce defects that hinder charge mobility. GO's moderate conductivity, coupled with its tunable reduction during synthesis, allows for optimization of both charge transport and ZnO coupling efficiency. ZnO/GO nanocomposites possess outstanding properties, including high surface area, excellent electrical conductivity, and remarkable thermal stability, making them ideal candidates for photocatalysis [14].

Various synthesis techniques, including sol-gel [15], hydrothermal [16], sonication [17], and microwave-assisted reactions [18], have been explored to fabricate ZnO/GO nanocomposites, each providing unique advantages. This research aims to investigate the role of modified microwave reactor heating in the synthesis of ZnO/GO nanocomposites, with a particular focus on assessing their efficiency in MB dye degradation compared to conventional heating methods.

Materials and methods

Materials

The materials used in this study include graphite fine powder extra pure, zinc nitrate ($Zn(NO_3)_2$, 99 %, p.a.), ammonium hydroxide (NH_4OH, 25 %, p.a.), sodium nitrate ($NaNO_3$, 99 %, p.a.), sulfuric acid (H_2SO_4, 98 %, p.a.), hydrochloric acid (HCl, 37 %, p.a.), potassium permanganate ($KMnO_4$, 99 %, p.a.), hydrogen peroxide (H_2O_2, 30 %, p.a.), and methylene blue (p.a.). All analytical-grade (p.a.) chemicals were

purchased from Merck and used without further purification.

Methods

Synthesis of ZnO

Initially, 20 g of $Zn(NO_3)_2$ was dissolved in 100 mL of deionized water. The solution was then precipitated by gradually adding NH_4OH to reach a pH of 8, followed by a washing process with deionized water to achieve a neutral pH. For the conventional heating method, the resulting precipitate was heated in an oven at 200 °C for 2 hours. In the microwave heating method, a microwave modified reactor was used for 10 minutes.

Synthesis of GO

GO was synthesized using a modified Hummers method, as described in our previous work in Agusu *et al.* [19]. Two grams of graphite powder were added to 98 mL of H_2SO_4 containing 4 g of $NaNO_3$, then cooled in an ice bath for 1 hours while stirring vigorously. Next, 8 g of $KMnO_4$ was added gradually while maintaining the temperature at 0 °C. After stirring at room temperature for 20 hours, the solution turned dark brown. Subsequently, 200 mL of deionized water was added drop by drop while keeping the temperature below 50 °C, followed by the slow addition of 20 mL of H_2O_2. When the color turned brownish-black, HCl was added to remove the remaining metal ions. The mixture was then washed with deionized water until the pH was neutral and dried in an oven at 105 °C for 12 hours.

Synthesis of ZnO/GO nanocomposites

A total of 0.24 g of ZnO and 0.08 g of GO were dispersed in 80 mL of deionized water, resulting in a suspension that was subsequently placed in a Teflon-lined autoclave. The autoclave was heated in an oven at 160 °C for a duration of 12 hours. Following this process, the suspension was dried at 105 °C for 3 hours. The ZnO/GO composite was subsequently prepared through conventional heating at 200 °C for 2 hours. Additionally, a ZnO/GO sample was synthesized utilizing modified microwave reactor heating for 10 minutes.

Characterization

X-ray diffraction (XRD, Rigaku Smart Lab) analysis was performed on powder samples scanned from 10º to 80° (2θ) at a rate of 2° per minute with a step size of 0.02° to determine phase purity and crystallite size. Fourier transform infrared (FTIR, Shimadzu IRPrestige-21) spectroscopy was conducted using KBr pellets (1:100 sample:KBr ratio) across 400 to 4,000 cm^{-1} at a resolution of 4 cm^{-1} resolution. Field Emission Scanning Electron Microscopy (FESEM, JSM-IT 700HR) was operated at 5 to 15 kV with a resolution of 1.0 nm to examine surface morphology. Optical properties and photocatalytic performance were analyzed using a UV-Vis spectrophotometer (Genesis 150) in diffuse reflectance mode (200 to 800 nm).

Photocatalytic experiments

The photocatalytic degradation process using ZnO and ZnO/GO nanocomposites was conducted under UV (365 nm, 10 mW/cm^2) and visible light (420 - 700 nm, 50 mW/cm^2) irradiation with a 300 W Xenon lamp with appropriate filters. The reaction progress was monitored via UV-Vis spectrophotometry by measuring the absorbance of MB at a wavelength of 664 nm. A total of 10 mg of each ZnO and ZnO/GO was used as photocatalysts in 10 mL of MB solution with a concentration of 10 ppm. Degradation rate measurements were taken at 10, 20, 30, 40, and 50 minutes.

Results and discussion

X-ray diffraction analysis

The XRD patterns of ZnO and ZnO/GO synthesized with two heating processes are presented in **Figure 1**. ZnO exhibits distinct peaks at 2θ = 31.7, 34.4, 36.3, 47.5, 56.5, 62.9, 66.4, 68.0, and 69.1°, corresponding to the crystal planes (100), (002), (101), (102), (110), (103), (200), (112), and (201), respectively. These peaks align with Crystallography Open Database (COD) No. 00-900-4180, confirming the hexagonal wurtzite structure of ZnO with a space group of P63mc (#63-1). In contrast, the diffraction peak of GO at 11.0° corresponds to the (001) plane of the hexagonal crystal structure of GO, as reported by Alkhouzaam *et al.* [20]. The results of the crystallite size analysis presented in **Table 1**, calculated using the Scherrer (Eq**. (1)**).

$$D = \frac{k\lambda}{\beta \cos\theta} \quad (1)$$

where D, k, λ, β, and θ are the average particle size, coupling constant ($k = 0.9$), the wavelength of the X-ray (λ = 1.54056 Å), the full width at half-maximum (FWHM), and the Bragg angle, respectively [21]. FWHM was determined by fitting the (101) diffraction peak with a Gaussian function.

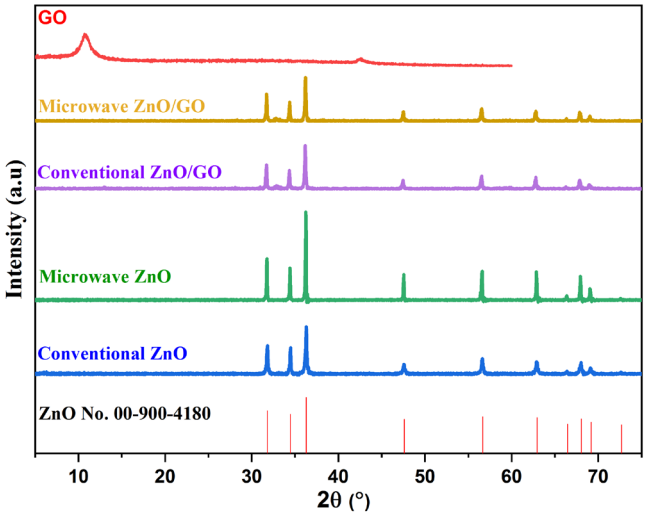

XRD patterns of ZnO and ZnO/GO synthesized with different heating processes.

Modified microwave reactor heating produced significantly larger crystal sizes (90.3 nm for ZnO and 55.6 nm for ZnO/GO) compared to conventional heating. This difference can be attributed to the increase in temperature, which is influenced by the loss tangent (tan δ = ε”/ε’) where ε’ and ε” represent the real and imaginary components of the permittivity constant, respectively. In the work of Yuwen *et al.* [22], GO has a lower tan δ value (about 0.03) than ZnO (about 0.0529) as reported by Horikoshi *et al.* [23]. The lower tan δ value of GO results in less efficient absorption of microwave energy, thereby slowing down the heating process and consequently limiting the growth rate of ZnO particles in the ZnO/GO composite. Nonetheless, the crystal size of modified microwave reactor heated ZnO/GO is still larger than that of conventional heating, although, the difference is not very noticeable compared to pure ZnO.

Other information from **Table 1** includes the crystalline parameters of hexagonal ZnO, namely *a* and *c*. These parameters are extracted through Rietveld refinement. The c/a ratio for ZnO, whether calcined via conventional heating or microwave radiation, is consistently 1.6013, which is still much lower than the ideal value of 1.633 stated by Özgür *et al.* [24]. This lower c/a ratio indicates the presence of unit cell compression along the c-axis (vertical axis), suggesting that the hexagonal structure is not perfectly aligned and the crystal lattice undergoes ‘squeezing’ in the vertical direction. Conversely, the incorporation of GO increased the c/a ratio (1.6020 for conventional heating and 1.6023 for microwave heating), indicating that modified microwave reactor heating and the addition of GO promote further expansion of the ZnO crystal along the z-axis.

Table 1 Summarized XRD data analysis.

Space Group: P63mc (186-1)				
Treatment	**Microwave**		**Conventional**	
Materials	**ZnO**	**ZnO/GO**	**ZnO**	**ZnO/GO**
a (Å)	3.2519	3.2557	3.2539	3.2550
c (Å)	5.2072	5.2165	5.2105	5.2145

Space Group: P63mc (186-1)				
Treatment	**Microwave**		**Conventional**	
Materials	**ZnO**	**ZnO/GO**	**ZnO**	**ZnO/GO**
c/a	1.6013	1.6023	1.6013	1.6020
V(Å^3)	47.6889	47.8861	47.7781	47.8454
D (nm)	90.3	55.6	44.3	49.3

The absence of the GO diffraction peak in **Figure 1** at around 11.0° indicates that the ZnO group effectively prevents the re-stacking of graphene layers. ZnO acts as a spacer, ensuring that each graphene sheet remains well separated. This observation is consistent with the findings of Kumar *et al.* [25]. Moreover, it also indicates that GO has been completely exfoliated and uniformly dispersed within the ZnO nanoparticles. The incorporation of GO did not change the wurtzite crystal structure of ZnO, likely due to the minimal amount of GO added and the reduced interference with the graphene layer caused by the ZnO intercalation, similar to the work of Sayem *et al.* [26].

As reported by Kachere *et al.* [27], although different heating techniques lead to variations in diffraction peak intensity, samples heated using microwaves exhibit higher peak intensities. This indicates that microwave heating produces crystalline structures of superior quality, due to improved crystallinity and phase homogeneity. It was observed that conventionally heated ZnO showed a larger crystallite size compared to the ZnO/GO nanocomposite. This can be attributed to the interaction between ZnO nanoparticles and GO, which induces a restructuring process. The interaction promotes crystallite growth resulting in an overall increase in ZnO crystal size [28].

Microstructural analysis of ZnO nanoparticle

The microstructural analysis of ZnO nanoparticles aims to understand their physical characteristics, dislocation density, strain, stress, and energy density. This analysis is crucial for understanding the properties and potential applications of these nanoparticles in their application as high-performance methylene blue photocatalysis.

Dislocation density

Dislocation density is a measure of the number of dislocation line defects within crystalline material per unit volume or area. It is usually defined as the total length per unit volume, or equivalently, as the number of dislocations intersecting an area in a plane. The number crossing between 2 parallel surfaces divided by their separation. Dislocation density is a key material as parameter, since it has profound effects on the mechanical properties of materials such as strength and ductility**.** Dislocation density (δ_{den}) mathematically calculated using Equation $\delta_{den} = 1/D^2$ [29], where D represents crystallite size [30].

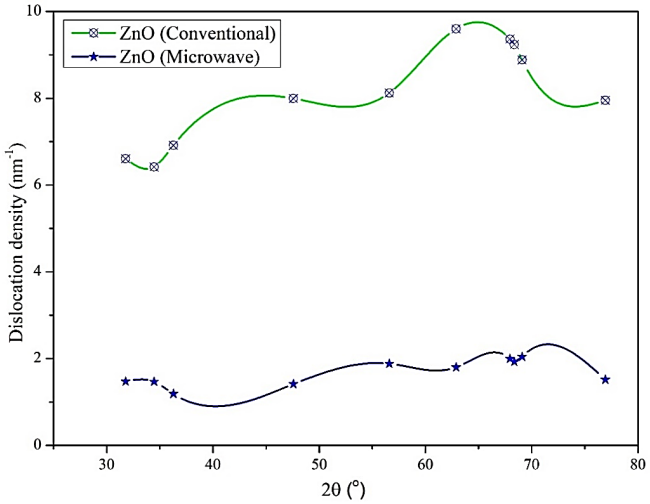

Figure 2 Dislocation density of ZnO nanoparticle synthesized with conventional and modified microwave reactor heating.

Figure 2 shows the calculated result of the dislocation density for ZnO nanoparticles synthesized using conventional and modified microwave reactor heating. Based on the calculations depicted in **Figure 2**, the dislocation density of ZnO nanoparticles synthesized by the conventional method is higher than that of those synthesized using the microwave heating method. These results indicate that ZnO nanoparticles produced by the modified microwave reactor method exhibit better quality compared to those synthesized by the conventional method. Consistent with the findings of Průša *et al.* [31], our study reveals a similar phenomenon.

Microstrain value

Microstrain is defined as a change in length divided by the initial length. Microstrain in materials refers to the ability of a material to withstand deformation under stress before certain permanent changes occur. It is a significant term in material strength, as it enables engineers to understand how materials behave under load and to construct structures that safely those loads. Microstrain a measures material deformation, typically expressed as the change in length over the original length, assuming that the microstrain of ZnO is uniform in all crystallographic directions, concept known as the uniform deformation model (UDM). The microstrain of ZnO nanoparticle value $\boldsymbol{\varepsilon}$ was estimated using Eq. (2) [29].

$$\beta \cos\theta = \frac{K\lambda}{D} + 4\varepsilon \sin\theta \quad (2)$$

where β is the corrected instrumental half-width of the maximum intensity broadening, K is the Scherrer constant, D is the crystal size of the ZnO nanoparticles, λ is the X-ray wavelength, and θ is diffraction angle.

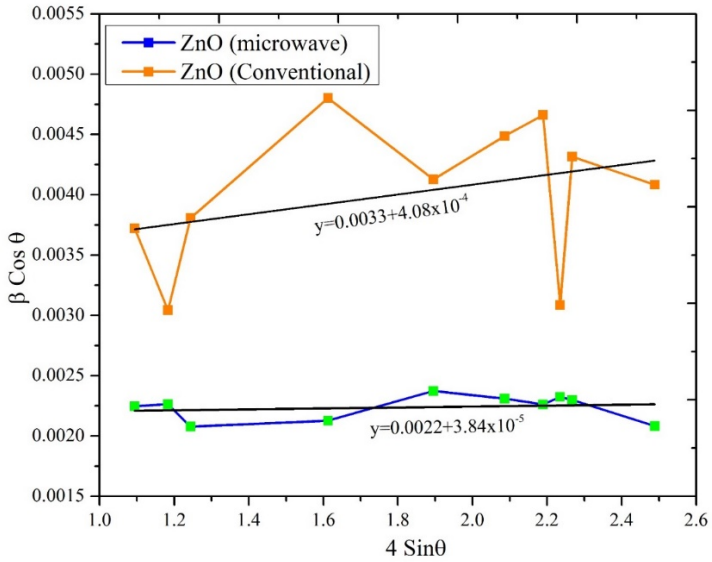

Figure 3 Strain value of ZnO nanoparticle synthesized with conventional and modified microwave reactor heating.

The values of $\beta \cos\theta$ on the y-axis were plotted as a function of 4 sin θ on the x-axis, and from the linear fit of the data, the microstrain $\boldsymbol{\varepsilon}$ was estimated from the slope of the linear fit (**Figure 3**). Based on the results shown in **Figure 3**, the microstrain for ZnO nanoparticles synthesized by the conventional method is 4.08×10^{-4}, while for those synthesized using the modified microwave reactor method is 3.84×10^{-5}. These results indicate that ZnO nanoparticles synthesized by the microwave method have a better crystal structure compared to those synthesized by the conventional method. This is also supported by the higher intensity of ZnO nanoparticles synthesized by the modified microwave reactor method, similar to the findings of Kumar *et al.* [32].

Stress value

The definition of stress involves how materials resist internal changes when forces act upon them from the outside. A material experiences stress as the force

per unit area that develops from any external load applied to it. Several fundamental principles of materials science engineering address stress, as it helps identify material behavior under stress and strain conditions for constructing safe long-lasting structures. The stress value of ZnO nanoparticles σ was estimated using Eq. (4) with the value of ε obtained from Eq. (3) [29].

$$\beta \cos\theta = \frac{K\lambda}{D} + 4\varepsilon \, sin\theta/Y \quad (3)$$

$$\sigma = \varepsilon . Y \quad (4)$$

where β is the corrected instrumental half-width of maximum intensity broadening, K is the Scherrer constant, D is the crystal size of the ZnO nanoparticle, λ is the X-ray wavelength, θ is the diffraction angle, and Y is Young's modulus.

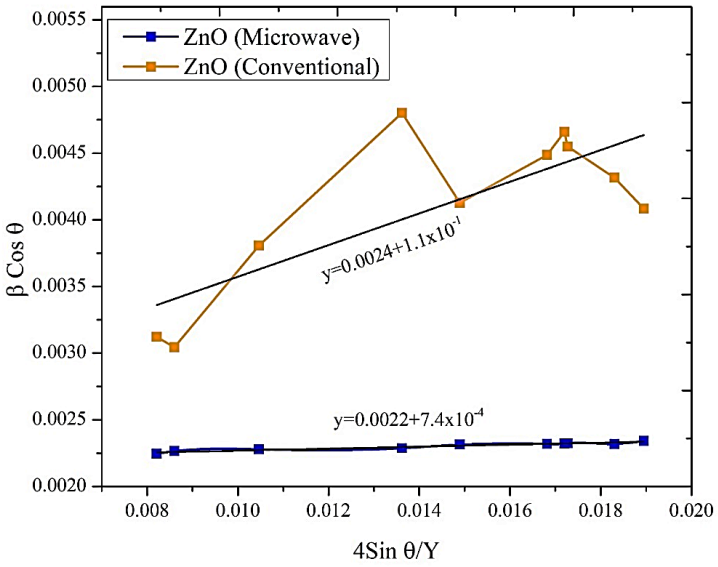

Figure 4 Stress value of ZnO nanoparticle synthesized with conventional and modified microwave reactor heating.

Figure 4 reveals a significant difference in residual stress between synthesis methods: ZnO nanoparticles prepared via conventional methods exhibit 0.11 MPa tensile stress, while those synthesized using the modified microwave reactor show drastically lower stress (7.4×10^{-4} MPa). This 150-fold reduction in stress strongly suggests improved crystal quality in the microwave-synthesized nanoparticles. The observed low-stress state is consistent with findings of Sutapa *et al.* [29] for MgO nanoparticles (a structurally analogous oxide system), where stress reduction correlated strongly with narrower crystallite size distributions and a more uniform lattice strain field. This agreement across oxide materials highlights the universal relationship between low residual stress and improved structural perfection. Furthermore, our results align precisely with Kumar *et al.* [32] Tohluebaji *et al.* [45], who demonstrated that microwave-assisted synthesis provides exceptional control over ZnO crystal growth. Their systematic study revealed that optimized microwave conditions produce hierarchical ZnO nanostructures with minimized lattice defects (e.g., vacancies and dislocations), thermodynamically stable growth conditions, and reduced thermal gradients that typically induce defect proliferation in conventional methods.

Energy density

Energy density refers to how energy is stored per unit volume or mass of matter. The reasons why nanoparticles have substantially enhanced energy density compared to bulk materials are mainly due to their elevated surface area-to-volume ratio and their distinctive electronic and physical properties. Because of these characteristics, they are especially attractive for use in energy storage devices and other applications [29,33]. To estimate the energy density values of ZnO nanoparticles synthesized by conventional and microwave heating, Eq. (3) was modified according to the energy and strain relation to become Eq. (5).

$$\beta \cos\theta = \frac{K\lambda}{D} + \left(4sin\theta \left(\frac{2E_{ed}}{Y}\right)^{1/2}\right) \quad (5)$$

Plots of $\beta \cos\theta$ versus $4sin\theta \left(\frac{2E_{ed}}{Y}\right)^{1/2}$ were constructed, and the data were fitted to lines (**Figure 5**). Based on the results shown in **Figure 5**, the energy density for ZnO nanoparticles synthesized by the conventional method is 1.22×10^{-7} kJ·m^{-3}, while that for the modified microwave reactor method is 5.10×10^{-7} kJ·m^{-3}. This suggests that the energy density for ZnO nanoparticles synthesized by the conventional method is lower than that of the modified microwave reactor method. The potential of ZnO nanoparticles is very beneficial for applications that involve the energy density of nanoparticles, such as photocatalytic materials [11,34].

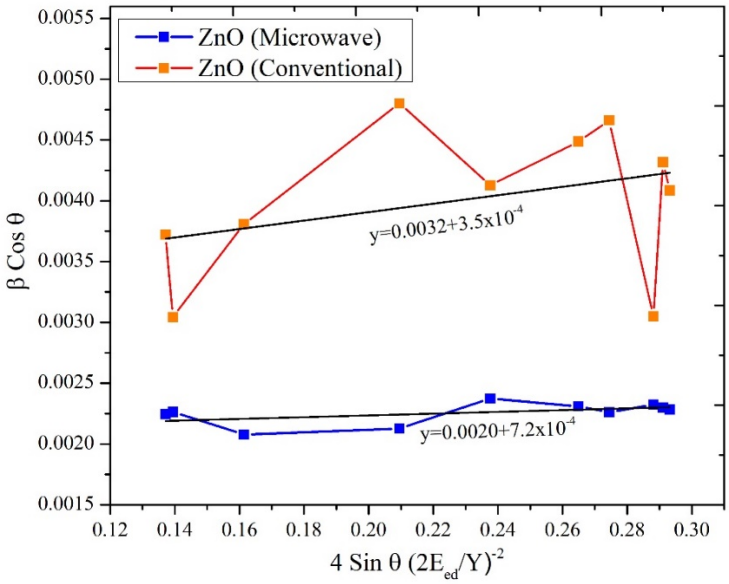

Figure 5 Energy density of ZnO nanoparticle synthesized with conventional and modified microwave reactor heating.

FTIR spectroscopy analysis

The FTIR spectra show no significant differences between the two heating methods, indicating that modified microwave reactor heating effectively maintains the stability of the functional groups in the material (**Figure 6**). The identified ZnO functional groups align with the results reported by [11,21], while the GO functional groups correspond to those described by [13,35]. A typical GO feature in ZnO/GO appears at wave numbers 1,641 - 1,647 cm^{-1}, corresponding to C=O/C=C stretching vibrations. Additionally, the peak at 3,381 - 3,385 cm^{-1} in ZnO/GO is attributed to hydroxyl groups present in both ZnO and GO. The incorporation of GO into ZnO resulted in the weakening of the peak around 522 cm^{-1} [35].

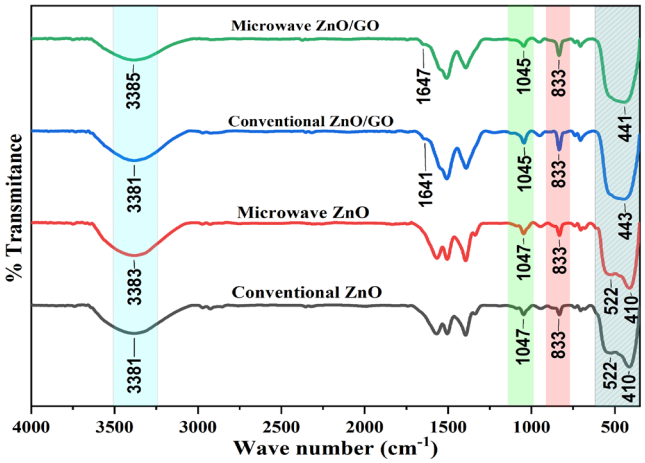

Figure 6 FTIR analysis results of ZnO and ZnO/ GO synthesized by conventional and modified microwave reactor heating.

FESEM analysis

The surface morphology of the FESEM analysis results is shown in **Figure 7**. In the case of conventional heating of ZnO (**Figure 7(a)**), the nanocrystalline flakes exhibit a flat and irregular morphology, consistent with the findings reported by Manikandan *et al.* [36]. In contrast, the ZnO nanoparticles synthesized under modified microwave reactor heating (**Figure 7(b)**) display a flat and regular flake shape with a more uniform distribution. **Figure 7(c)**, highlights that the surface of the GO sheet is effectively covered by ZnO crystals, indicating good integration between the GO sheet and ZnO nanoparticles. **Figure 7(d)**, shows that microwave heating causes the ZnO/GO to collapse into smaller sizes due to agglomeration, which contributes to an increase in specific surface area and enhances the photocatalytic performance. These observations align with the results reported by Lin *et al.* [37], using a different heating technique.

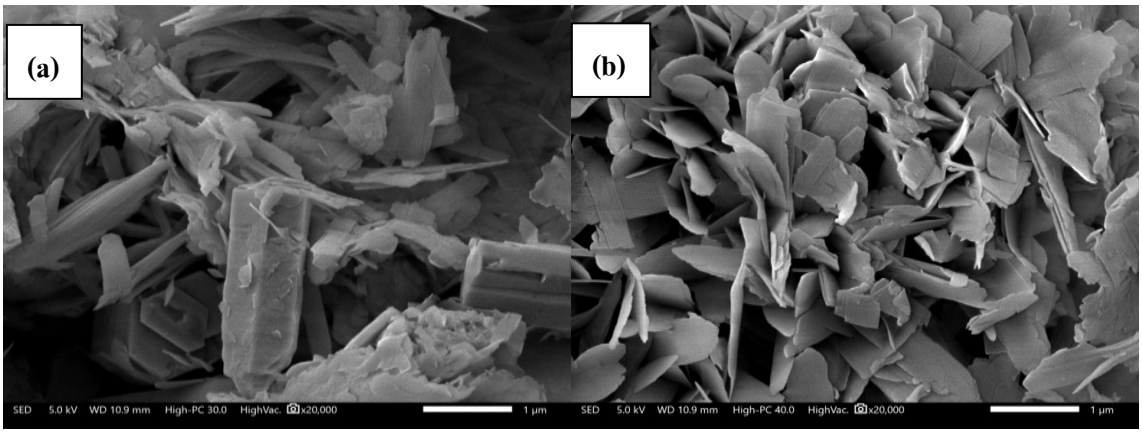

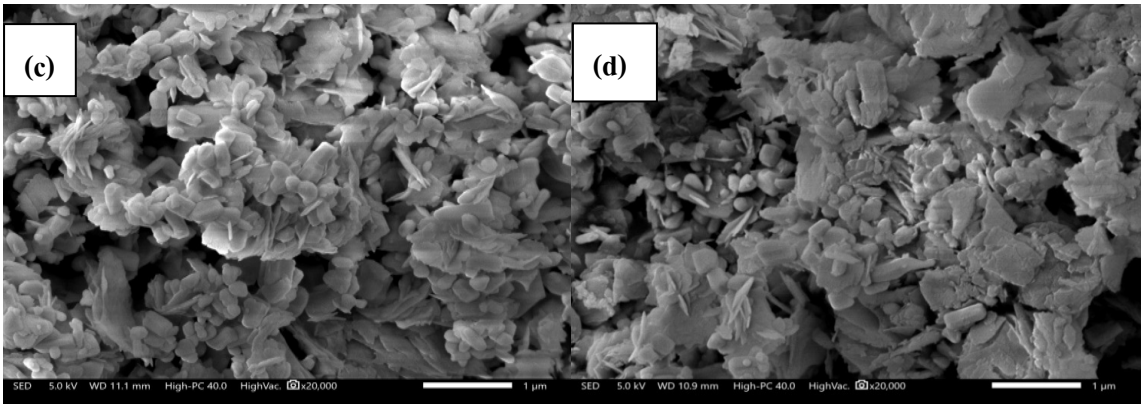

Figure 7 ZnO and ZnO/GO with conventional and microwave heating, (a) ZnO conventional, (b) ZnO microwave, (c) ZnO/GO conventional, and (d) ZnO/GO microwave.

The FESEM results (**Figure 7**) directly reflect the tan δ-governed nucleation dynamics. While graphene oxide (GO) typically exhibits a higher tan δ than ZnO due to its polar functional groups, certain conditions (e.g., low oxidation degree, high-frequency measurements, or solvent effects) can result in GO having a lower tan δ than ZnO. This implies nucleation and growth during microwave treatment due to a selective and local heating mechanism. In this context, ZnO, with its higher (higher tan δ) with stronger microwave absorption, ZnO precursors heat more efficiently, leading to rapid nucleation. Volumetric heating dominates, potentially resulting in homogeneous nanoparticle formation. It generates uniform flakes in **Figure 7(b)**. GO (lower tan δ) absorbs less microwave energy, localized heating at defect sites (e.g., residual sp^2 domains and edges) becomes critical. This may create limited but strategic hotspots where ZnO nucleation is favored due to interfacial interactions. The selective absorption mechanism may result in ZnO growth dominance because of the higher microwave susceptibility of ZnO precursors. This could lead to faster ZnO crystallization, while GO remains relatively inert, acting mainly as a template or a slow-reducing agent. Selective absorption may induce heterogeneous nucleation on the GO surface. Even with a lower tan δ, GO's residual conductive regions (small sp^2 clusters) or defects may still attract ZnO nanoparticles due to charge interactions between polar ZnO and GO's oxygen groups, as well as due to microwave-induced polarization at GO/ZnO interfaces, promoting oriented attachment. The subsequent collapse into agglomerates (**Figure 7(d)**) arises from late-stage microwave-driven reduction and interfacial polarization, creating photocatalytic-active sites. Conventional heating in **Figures 7(a)** and **7(b)** lacks such selectivity, yielding disordered morphologies.

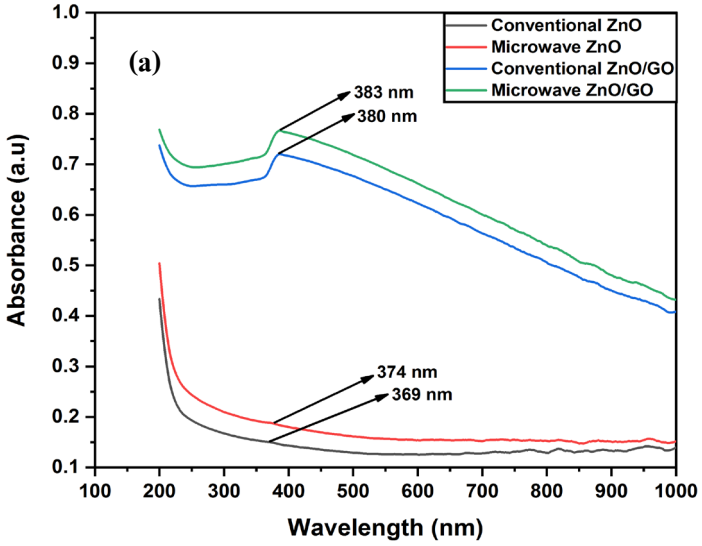

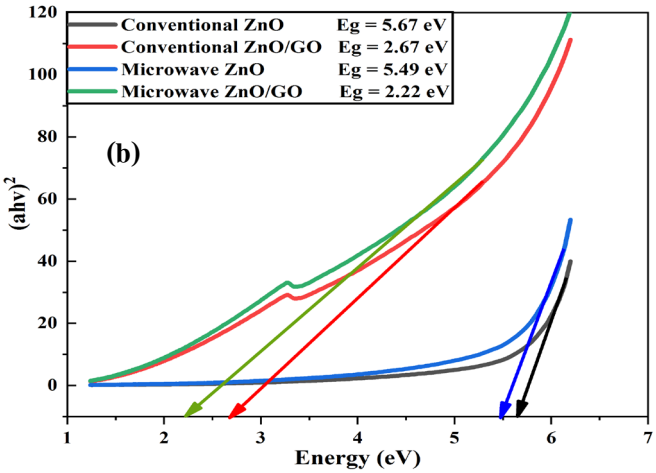

Figure 8 (a) Absorbance vs wavelength, and (b) Tauc's plots for ZnO and ZnO/GO nanocomposites.

UV-Vis spectrophotometer analysis

Optical characteristics of photocatalysts

The optical properties of ZnO and ZnO/GO nanocomposites plotted by absorbance vs wavelength and used to determine the band gap energy are shown in **Figure 8**. In **Figure 8(a)**, the absorption peaks for ZnO synthesized via conventional and modified microwave reactor methods are observed at 369 and 374 nm, respectively. After doping with GO, the absorption peaks of ZnO shifted from 383 and 380 nm for microwave and conventional heating, accompanied by a slight increase in light absorption intensity. This increase is due to the additional absorption contributed by GO, which increases the electric charge on the oxide surface and changes the process of electron-hole pair formation during irradiation. The integration of GO into ZnO not only enhances light absorption but also increases the active sites and electrical charges of the surface, leading to a higher absorption coefficient under light irradiation [37,38].

Figure 8(b) shows ZnO synthesized by conventional and modified microwave reactor heating exhibiting band gap energies of 5.67 and 5.49 eV. There is a shift of the absorption edge towards longer wavelengths corresponding to the reduction of band gap energy. After the incorporation of GO, the band gap energy decreased to reach 2.67 and 2.22 eV for conventional and microwave-synthesized ZnO/GO, respectively. The band gap energy was determined by the Tauc's plot through (Eq**. (6)).**

$$(\alpha hv)^n = A(hv - Eg) \quad (6)$$

here, α, hv, and A represent the absorption coefficient, photon energy, and characteristic constant of the material, respectively. The n is equal to 1/2 for indirect transitions and 2 for direct transitions. Eg can be found by extrapolating the linear portion of the $(\alpha hv)^2$ graph to the x-axis ($\alpha = 0$) [33].

The incorporation of GO reduces the band gap energy by reducing the Burstein-Moss effect, which shifts the absorption edge of the nanocomposite towards higher wavelengths. GO facilitates the movement of electrons to the π-system of GO, thus vacating the conduction band and lowering the Fermi level closer to the valence band, which enables better absorption of visible light [32,38]. These findings are in line with previous studies [39], which showed that integrating GO with ZnO increases the photocatalytic efficiency in the visible spectrum. The narrowed band gap is believed to allow more charge carriers to participate in the photocatalytic reaction [40]. It is important to note that this study produced pure ZnO with a larger band gap energy than typically observed. Khan *et al.* [41], explained that the band gap energy can vary depending on the precursor used, as it influences the final atomic ratios of C/N, O/C, and O/Zn in the ZnO samples. These variations in atomic composition, in turn, lead to differences in the band gap values. Additionally, Limón *et al.* [42] have provided valuable insights into the effect of ZnO precursors on band gap energy, which can serve as a foundational reference for understanding these variations.

Performance of photoactivity

The degradation ability of MB by ZnO and ZnO/GO was calculated according to (**Eq. (7)**, **Table 2**). ZnO/GO, when heated using microwave irradiation, achieved the highest degradation performance under UV and visible light, with removal efficiencies of 87.4% and 66.6%, respectively, after 50 minutes of exposure.

$$Pdeg\ (\%) = \frac{C_o - C_t}{C_o} \times 100 \quad (7)$$

Where, *Pdeg* refers to the photocatalytic degradation of MB, C_0 is the initial concentration of the MB solution, and C_t is the concentration of the MB solution at the irradiation time [34].

Table 2 Summary of the photocatalytic performance of ZnO/GO nanocomposites and pure ZnO in the degradation of MB.

Time	% Degradation							
	Conventional ZnO		Microwave ZnO		Conventional ZnO/GO		Microwave ZnO/GO	
	UV	Vis	UV	Vis	UV	Vis	UV	Vis
0	0	0	0	0	0	0	0	0
10	1.8	0.3	1.6	6.9	42.6	34.4	61.1	35.9
20	4.1	1.4	9.2	7.7	44.1	37.5	64.3	42.2
30	5.7	2.5	11.8	12.5	60.2	53.8	71.1	55.3
40	8.1	3.8	13.4	13.9	64.4	56.0	77.6	60.6
50	8.5	5.5	22.0	16.8	84.3	66.5	87.4	66.6

The real-time degradation efficiency of MB increased with longer irradiation times under UV and visible light, indicating excellent photocatalytic activity, as shown in **Figure 9**. **Figure 9(a)** illustrates that ZnO/GO exhibited superior MB degradation compared to pure ZnO (**Figure 9(b)**). The enhanced performance of the ZnO/GO composite can be attributed to the presence of GO, which increases the availability of active sites, enhances light absorption, promotes the formation of reactive oxygen species (ROS), and facilitates the formation of π-π interactions between the photocatalyst and dye molecules. In addition, GO aids in the transfer of photoexcited electrons from the ZnO conduction band to the GO network, reducing electron-hole recombination and extending the minority carrier diffusion length. This increases the photocurrent in the nanocomposite. As a result, the photocatalytic performance of GO-supported ZnO nanostructures is enhanced under UV light irradiation due to the synergistic effect between the strong visible light absorption of GO and the UV photocatalytic activity of ZnO [39,43].

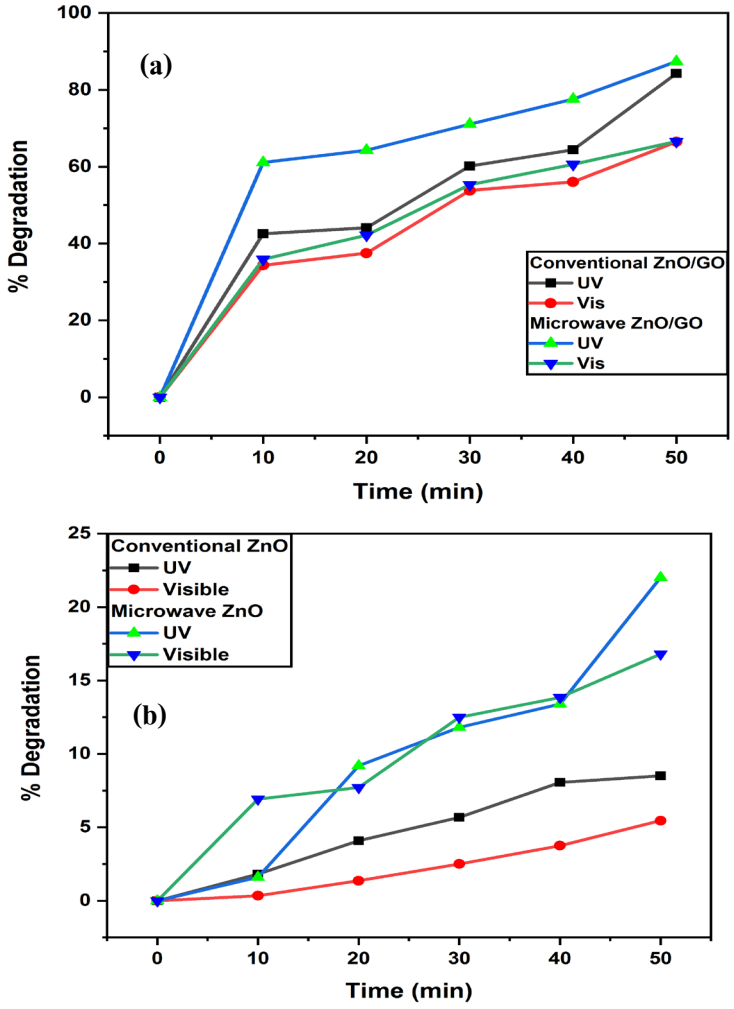

Figure 9 Photocatalytic performance of (a) ZnO/GO nanocomposites (b) pure ZnO.

Based on the experimental results, the proposed mechanism for the photocatalytic degradation of organic dyes using the ZnO/GO photocatalyst (**Figure 10**) follows the pathway suggested by Puneetha *et al.* [44].

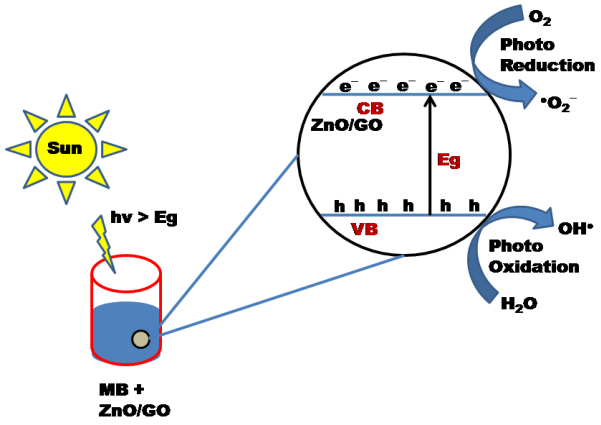

Figure 10 Photocatalytic degradation mechanism of MB dye.

Initially, MB dye adsorbs onto the surface of the ZnO/GO photocatalyst. Upon visible light irradiation, the ZnO/GO is excited, generating electron-hole pairs, with holes in the valence band (VB) and electrons in the conduction band (CB) of ZnO when the photon energy exceeds the band gap energy (hν > Eg) (Eq. (8)). The

photoinduced electrons are transferred to the GO nanosheets (Eq. (9)), effectively enhancing the separation of photogenerated charges. These electrons and holes react with O_2 and H_2O/OH^- in the solution, generating highly reactive oxidative species, such as superoxide anion radicals ($\bullet O_2^-$) and hydroxyl radicals ($\bullet$OH), as shown in Eqs**. (**10**)** and **(**11**).** These reactive species then degrade the MB molecules adsorbed on the catalyst surface, ultimately producing carbon dioxide (CO_2), water (H_2O), and other by-products (Eq. (12)).

$$ZnO / GO + h\nu \rightarrow ZnO_{CB}(e^-) + ZnO_{VB}(h^+) \quad (8)$$

$$ZnO_{CB}(e^-) + GO \rightarrow ZnO_{CB} + GO(e^-) \quad (9)$$

$$GO(e^-) + O_2 \rightarrow GO + \bullet O_2^- \quad (10)$$

$$ZnO_{VB}(h^+) + H_2O \rightarrow ZnO_{VB} + \bullet OH \quad (11)$$

$$MB + \bullet O_2^- + \bullet OH \rightarrow CO_2 + H_2O + \text{Intermediates} \quad (12)$$

Conclusions

The modified microwave reactor heating method produced ZnO nanoparticles with superior crystallinity and more uniform morphology. The microstructural analysis results show that the dislocation density, microstrain, and stress value of ZnO nanoparticles synthesized by the conventional method are higher than those of the modified microwave reactor method, while the energy density of ZnO nanoparticles synthesized by the conventional method is lower than that of the modified microwave reactor method. The incorporation of GO promotes better dispersion of ZnO nanoparticles, overcoming the limitations of pure ZnO, such as electron-hole recombination, while also contributing to band gap reduction. The ZnO/GO nanocomposite has a band gap energy of 2.22 eV for the modified microwave reactor method, which is superior to that of conventional heating (2.67 eV). The degradation of MB reached 87.4% and 66.6% under UV and visible light, respectively, after 50 min. Modified microwave reactor-assisted synthesis combined with GO integration is an effective strategy for developing high-performance photocatalysts with enhanced photocatalytic activity under UV and visible light irradiation.

Acknowledgements

We want to extend our heartfelt appreciation for the valuable support provided through the collaboration between Universitas Halu Oleo, Indonesia, and the University of Fukui, Japan. This research was partially supported by the Agreement on the Cross-Appointment System for Foreign Academic Staff (CA-FY2023) at the University of Fukui. Mr. La Ode Muhammad Darusman would also like to express his sincere gratitude for the Travel Grant for Young Researchers from the University of Fukui in FY2023.

Declaration of Generative AI in Scientific Writing

The authors acknowledge the use of generative artificial intelligence tools (e.g., editGPT) in language editing and grammar correction. No content generation or data interpretation was performed by artificial intelligence. The authors are solely responsible for the content and conclusions of this work.

CRediT Author Statement

La Agusu: Conceptualization, Methodology, Supervision, Validation, Funding acquisition, and Writing–original draft.

La Ode Muhammad Darusman: Data curation, Formal analysis, Investigation, Validation, and Visualization.

Alimin: Formal analysis, Investigation, Validation, and Visualization.

La Ode Kadidae: Data curation, Formal analysis, Validation, and Visualization.

Ahmad Zaeni: Data curation, Validation, and Visualization.

La Ode Ahmad: Supervision, Validation, and Writing–original draft.

Fadel Muhamad: Conceptualization, Resources, Software, and Writing–review & editing.

I Wayan Sutapa: Validation, Visualization and Writing –review & editing.

Yuya Ishikawa: Data curation, Formal analysis, and Investigation.

Kohei Nakagawa: Data curation, Formal analysis, and Investigation.

Yutaka Fujii: Data curation, Formal analysis, and Investigation.

Takayuki Asano: Supervision, Validation, and Writing –original draft.

Seitaro Mitsudo: Conceptualization, Resources, Funding acquisition, and Writing–review & editing.

References

[1] M Berradi, R Hsissou, M Khudhair, M Assouag, O Cherkaoui, A El Bachiri and A El Harfi. Textile finishing dyes and their impact on aquatic environs. *Heliyon* 2019; **5(11)**, e02711.

[2] S Modi, VK Yadav, A Gacem, IH Ali, D Dave, SH Khan, KK Yadav, S Rather, Y Ahn, CT Son and BH Jeon. Recent and emerging trends in remediation of methylene blue dye from wastewater by using zinc oxide nanoparticles. *Water* 2022; **14(11)**, 1749.

[3] PO Oladoye, TO Ajiboye, EO Omotola and OJ Oyewola. Methylene blue dye: Toxicity and potential elimination technology from wastewater. *Results in Engineering* 2022; **16**, 100678.

[4] MF Zainuddin, NH Nik Raikhan, NH Othman and WFH Abdullah. Synthesis of reduced Graphene Oxide (rGO) using different treatments of Graphene Oxide (GO). *IOP Conference Series: Materials Science and Engineering* 2018; **358**, 012046.

[5] Y Sun and DW O'Connell. Application of visible light active photocatalysis for water contaminants: A review. *Water Environment Research* 2022; **94(10)**, e10781.

[6] F Jamal, A Rafique, S Moeen, J Haider, W Nabgan, A Haider, M Imran, G Nazir, M Alhassan, M Ikram, Q Khan, G Ali, M Khan, W Ahmad and M Maqbool. Review of metal sulfide nanostructures and their applications. *ACS Applied Nano Materials* 2023; **6(9)**, 7077-7106.

[7] RH Waghchaure, VA Adole and BS Jagdale. Photocatalytic degradation of methylene blue, rhodamine B, methyl orange and Eriochrome black T dyes by modified ZnO nanocatalysts: A concise review. *Inorganic Chemistry Communications* 2022; **143**, 109764.

[8] AF Abdulrahman and NM Abd-Alghafour. Synthesis and characterization of ZnO nanoflowers by using simple spray pyrolysis technique. *Solid-State Electronics* 2022; **189**, 108225.

[9] F Asjadi and M Yaghoobi. Characterization and dye removal capacity of green hydrothermal synthesized ZnO nanoparticles. *Ceramics International* 2022; **48(18)**, 27027-27038.

[10] S Arya, P Mahajan, S Mahajan, A Khosla, R Datt, V Gupta, SJ Young and SK Oruganti. Review-influence of processing parameters to control morphology and optical properties of sol-gel synthesized ZnO nanoparticles. *ECS Journal of Solid State Science and Technology* 2021; **10**, 023002.

[11] N Pauzi, N Mat Zain and NA Ahmad Yusof. Microwave-assisted synthesis of ZnO nanoparticles stabilized with gum arabic: Effect of microwave irradiation time on ZnO nanoparticles size and morphology. *Bulletin of Chemical Reaction Engineering & Catalysis* 2019; **14(1)**, 182-188.

[12] A Kulis-Kapuscinska, M Kwoka, MA Borysiewicz, T Wojciechowski, N Licciardello, M Sgarzi and G Cuniberti. Photocatalytic degradation of methylene blue at nanostructured ZnO thin films. *Nanotechnology* 2023; **34**, 155702.

[13] LF Madeo, C Schirmer, G Cirillo, AN Asha, R Ghunaim, S Froeschke, D Wolf, M Curcio, P Tucci, F Iemma, B Büchner, S Hampel and M Mertig. ZnO-graphene oxide nanocomposite for paclitaxel delivery and enhanced toxicity in breast cancer cells. *Molecules* 2024; **29(16)**, 3770.

[14] A Negash, S Mohammed, HD Weldekirstos, AD Ambaye and M Gashu. Enhanced photocatalytic degradation of methylene blue dye using eco-friendly synthesized rGO@ZnO nanocomposites. *Scientific Reports* 2023; **13(1)**, 22234.

[15] S Aydogan, N Canpolat, A Kocyigit and M Yilmaz. Synergistic enhancement of simazine degradation using ZnO nanosheets and ZnO/GO nanocomposites: A sol-gel synthesis approach. *Ceramics International* 2024; **50(14)**, 25080-25094.

[16] T Mahmood and F Baig. A comparative study of ZnO, ZnO/GO and ZnO/RGO nanocomposites for the energy application. *Research Square* 2024. https://doi.org/10.21203/rs.3.rs-4462456/v1

[17] S Víctor-Román, E García-Bordejé, J Hernández-Ferrer, JM González-Domínguez, A Ansón-

Casaos, AMT Silva, WK Maser and AM Benito. Controlling the surface chemistry of graphene oxide: Key towards efficient ZnO-GO photocatalysts. *Catalysis Today* 2020; **357(2020)**, 350-360.

[18] R Sánchez-Albores, FJ Cano, PJ Sebastian and O Reyes-Vallejo. Microwave-assisted biosynthesis of ZnO-GO particles using orange peel extract for photocatalytic degradation of methylene blue. *Journal of Environmental Chemical Engineering* 2022; **10(6)**, 108924.

[19] L Agusu, LO Ahmad, Alimin, Herdianto, S Mitsudo and H Kikuchi. Hydrothermal synthesis of reduced graphene oxide using urea as reduction agent: Excellent X-band electromagnetic absorption properties. *IOP Conference Series: Materials Science and Engineering* 2018; **367**, 012002.

[20] A Alkhouzaam, H Qiblawey and M Khraisheh. Polydopamine functionalized graphene oxide as membrane nanofiller: Spectral and structural studies. *Membranes* 2021; **11(2)**, 1-17.

[21] T Ivanova, A Harizanova, T Koutzarova, B Vertruyen and R Closset. Deposition of sol-gel ZnO:Mg films and investigation of their structural and optical properties. *Materials* 2022; **15(24)**, 8883.

[22] C Yuwen, B Liu, L Zhang, S Guo and J Peng. Synthesis high-quality graphene oxide and temperature-dependent dielectric properties of reduced graphene oxide. *Materials Research Express* 2019; **6(9)**, 0950b4.

[23] S Horikoshi, A Matsubara, S Takayama, M Sato, F Sakai, M Kajitani, M Abe and N Serpone. Characterization of microwave effects on metal-oxide materials: Zinc oxide and titanium dioxide. *Applied Catalysis B: Environmental* 2010; **99(3-4)**, 490-495.

[24] Ü Özgür, YaI Alivov, C Liu, A Teke, MA Reshchikov, S Doğan, V Avrutin, SJ Cho and H Morkoç. A comprehensive review of ZnO materials and devices. *Journal of Applied Physics* 2005; **98(4)**, 041301.

[25] P Kumar, S Som, MK Pandey, S Das, A Chanda and J Singh. Investigations on optical properties of ZnO decorated graphene oxide (ZnO@GO) and reduced graphene oxide (ZnO@r-GO). *Journal of Alloys and Compounds* 2018; **744**, 64-74.

[26] MA Sayem, MAH Suvo, IM Syed and MA Bhuiyan. Effective adsorption and visible light driven enhanced photocatalytic degradation of rhodamine B using ZnO nanoparticles immobilized on graphene oxide nanosheets. *Results in Physics* 2024; **58**, 107471.

[27] AR Kachere, PM Kakade, AR Kanwade, P Dani, N Kumar, TM Lik, SR Rondiya, NY Dzade, S Esh, R Jadkar and SV Bhosale. Zinc oxide/graphene oxide nanocomposites: Synthesis, characterization and their optical properties. *ES Materials & Manufacturing* 2021; **16**, 19-29.

[28] K Madi, D Chebli, H Ait Youcef, H Tahraoui, A Bouguettoucha, M Kebir, J Zhang and A Amrane. Green fabrication of ZnO nanoparticles and ZnO/rGO nanocomposites from Algerian date syrup extract: Synthesis, characterization, and augmented photocatalytic efficiency in methylene blue degradation. *Catalysts* 2024; **14(1)**, 62.

[29] IW Sutapa, A Wahid Wahab, P Taba and NL Nafie. Dislocation, crystallite size distribution and lattice strain of magnesium oxide nanoparticles. *Journal of Physics: Conference Series* 2018; **979**, 012021.

[30] J Gallet, M Perez, R Guillou, C Ernould, C Le Bourlot, C Langlois, B Beausir, E Bouzy, T Chaise and S Cazottes. Experimental measurement of dislocation density in metallic materials: A quantitative comparison between measurements techniques (XRD, R-ECCI, HR-EBSD, TEM). *Materials Characterization* 2023; **199**, 112842.

[31] D Průša, K Šuhajda, T Žajdlík, K Svobodová, S Šťastník, K Hobzova and V Venkrbec. Effect of microwave radiation on the compressive strength of solid ceramic brick. *Buildings* 2023; **13(4)**, 1018.

[32] R Kumar, RK Singh, DP Singh, R Savu and SA Moshkalev. Microwave heating time dependent synthesis of various dimensional graphene oxide supported hierarchical ZnO nanostructures and its photoluminescence studies. *Materials & Design* 2016; **111(A)**, 291-300.

[33] A Alimin, F Muhamad, A Alham, FN Adman, I Anjani, DA Amal, R Rahmayanti, LO Ahmad, F Fahmiati, A Zaeni, L Agusu, MZ Firihu, I Usman, SJ Santosa and AA Umar. A high-performance

supercapacitor electrode material based on carbon quantum dots originated from bamboo leaves of Southeast Sulawesi doped with nano magnetite derived from iron sands. *Materials Chemistry and Physics* 2025; **332**, 130151.

[34] H Ahmad Rafaie, NF Mohd Yusop, NF Azmi, NS Abdullah and NIT Ramli. Photocatalytic degradation of methylene blue dye solution using different amount of ZnO as a photocatalyst. *Science Letters* 2021; **15(1)**, 1-12.

[35] NF Norapandi, N Salim, KF Chong and NH Abu Bakar. Structural evaluation of graphene oxide/zinc oxide nanocomposite for corrosion mitigation. *Materials Today: Proceedings* 2023; **75(1)**, 58-62.

[36] B Manikandan, T Endo, S Kaneko, KR Murali and R John. Properties of sol gel synthesized ZnO nanoparticles. *Journal of Materials Science: Materials in Electronics* 2018; **29(11)**, 9474-9485.

[37] Y Lin, R Hong, H Chen, D Zhang and J Xu. Green synthesis of ZnO-GO composites for the photocatalytic degradation of methylene blue. *Journal of Nanomaterials* 2020; **2020(1)**, 4147357.

[38] M Karyaoui, DB Jemia, M Daoudi, A Bardaoui, A Boukhachem, M Amlouk and R Chtourou. Physical properties of graphene oxide GO-doped ZnO thin films for optoelectronic application. *Applied Physics A* 2021; **127**, 134.

[39] SA Al-Zahrani, K Umar, SA Tweib, JAM Rashd, SK Afridi, SA Bhawani, AA Otaibi, N Masood, D Mansour, A Khan and M Ayyar. Biomass mediated synthesis of ZnO and ZnO/GO for the decolorization of methylene blue under visible light source. *Catalysts* 2023; **13(2)**, 409.

[40] F Yildirim, N Canpolat, S Aydogan and M Yilmaz. Investigating the synergistic effect of ZnO/GO nanocomposite films for methylene blue removal. *Journal of the American Ceramic Society* 2024; **107(9)**, 6091-6107.

[41] SH Khan, B Pathak and MH Fulekar. Development of zinc oxide nanoparticle by sonochemical method and study of their physical and optical properties. *AIP Conference Proceedings* 2016; **1724**, 020108.

[42] I Limón-Rocha, CA Guzmán-González, LM Anaya-Esparza, R Romero-Toledo, JL Rico, OA González-Vargas and A Pérez-Larios. Effect of the precursor on the synthesis of ZnO and its photocatalytic activity. *Inorganics* 2022; **10(2)**, 16.

[43] J Chen, Y Xiong, M Duan, X Li, J Li, S Fang, S Qin and R Zhang. Insight into the synergistic effect of adsorption-photocatalysis for the removal of organic dye pollutants by Cr-doped ZnO. *Langmuir* 2020; **36(2)**, 520-533.

[44] J Puneetha, N Kottam and A Rathna. Investigation of photocatalytic degradation of crystal violet and its correlation with bandgap in ZnO and ZnO/GO nanohybrid. *Inorganic Chemistry Communications* 2021; **125**, 108460.

[45] N Tohluebaji, R Siri, N Muensit, C Putson, P Channuie, P Porrawatkul and J Yuennan. Hydrophobic and optical properties of P(VDF-HFP) nanofiber filled with Nickel (II) Chloride Hexahydrate for dye-sensitized solar cells application. *Trends in Sciences* 2024; **21(9)**, 2-28.